

Syntheses, Crystal Structures and Photophysical Properties of Two Doubly μ -Phenoxo-Bridged Ln^{III} (Ln = Pr, Nd) Homodinuclear Schiff Base Complexes

Joy Chakraborty,^[a] Santarupa Thakurta,^[a] Guillaume Pilet,^[b] Raymond F. Ziessel,^[c]
Loïc J. Charbonnière,^[c,d] and Samiran Mitra*^[a]

Keywords: Lanthanides / Schiff bases / Luminescence / Photophysics

Two novel homodinuclear isomorphous lanthanide(III) complexes [Ln(api)]₂ (where Ln = Pr and Nd for **1** and **2**, respectively) with Schiff base anion api³⁻ {H₃api = 2-(2-hydroxyphenyl)-1,3-bis[4-(2-hydroxyphenyl)-3-azabut-3-enyl]-1,3-imidazolidine} have been synthesized by a direct reaction of the Schiff base ligand and the corresponding hydrated lanthanide(III) nitrates in methanol. The geometry of each Ln^{III} ion in both complexes is distorted square antiprism (DSAP) as revealed by single-crystal X-ray diffraction studies and the structures are found to be centrosymmetric. Both the com-

plexes along with the ligand have been characterized by microanalysis and different spectroscopic techniques. A detailed photophysical investigation has been performed on both the ligand and the complexes. The fluorescence lifetime for the ligand is in the nanosecond regime, suggesting emission from a singlet state. The two lanthanide complexes exhibit NIR luminescence which has been explored through solid-state photoluminescence.

(© Wiley-VCH Verlag GmbH & Co. KGaA, 69451 Weinheim, Germany, 2009)

Introduction

Luminescent lanthanide (Ln) complexes have attracted a great deal of attention over many years due to their potential use in numerous analytical applications.^[1] Interest in the photophysical properties of lanthanide ion complexes has grown significantly since Lehn^[2] proposed that such complexes could be seen as light conversion molecular devices (LCMDs). From then, the design of efficient lanthanide complexes has become an important research goal, being pursued by several research groups, working with many different classes of ligands (e.g. chelating ligands,^[3–8] podands,^[9,10] calixarenes,^[11] macrocyclic ligands,^[9,12] β -diketonates,^[13] heterobiaryl ligands,^[14] carboxylic acid derivatives,^[15] terphenyl ligands,^[16] proteins^[17] etc.). Most of the complexes investigated, emit red or green light (Eu³⁺ and Tb³⁺ luminescence, respectively), but there are also complexes of different Ln³⁺ ions that luminesce in other spectral

regions: near-IR (Yb³⁺, Nd³⁺, Er³⁺),^[18] orange (Sm³⁺),^[16,19–21] yellow (Dy³⁺),^[16,22,23] blue (Tm³⁺)^[24] or near-UV (Ce³⁺,^[25] Gd³⁺)^[26]. Efficient LCMDs may find several applications, such as luminescent probes in biomedical assays,^[27] fluorescent lighting,^[28] luminescent sensors for chemical species (H⁺, O₂, halide ions, OH⁻),^[29] electroluminescent devices,^[30] UV dosimeters, or antireflection coatings for solar cells.^[31] The study of NIR luminescence is of much interest because the emission around 900–1600 nm, which is highly transparent to biological systems and fiber media, is valuable for time-resolved fluoro-immunoassay^[27] and optical telecommunication. In this respect, macrocyclic Schiff base ligands have gained immense favor due to both of their relatively straightforward synthesis and their multidentate encapsulating nature which results in very high binding constants for many *d*- and *f*-block metals.^[32] Hence there has been growing interest on dinuclear *3d–4f* and *4f–4f* complexes, which may exhibit such interesting properties. Currently, dinuclear *3d–4f* Schiff base complexes have been employed as building blocks to form extended structure,^[33] *2p–3d–4f*^[34] and *3d–3d'–4f* systems.^[35]

However, factors governing the formation of Ln³⁺–Ln³⁺ couples and their subsequent entrapment by dinucleating chelates remain largely obscure. Small changes in metal ionic radius and steric modifications at various sites on the Schiff base periphery produce marked changes on the dinuclear metal coordination geometries. With phenolic ligands the importance of a large chelate negative charge to lanthanide(III) ion ratio (ρ) to the dinucleation process was indicated by the greater stability of acyclic dinuclear complexes [LnL(NO₃)₂], in which $\rho = 2:1$, compared to dinuclear

[a] Department of Chemistry, Jadavpur University, Kolkata - 700 032, India
Fax: +91-33-2414 6414
E-mail: smitra_2002@yahoo.com

[b] Groupe de Cristallographie et Ingénierie Moléculaire, Laboratoire des Multimatériaux et Interfaces, UMR 5615 CNRS, Université Claude Bernard Lyon 1, Bât. Jules Roulin, 43 Bd du 11 Novembre 1918, 69622 Villeurbanne Cedex, France

[c] Laboratoire de Chimie Organique et Spectroscopies Avancées, UMR 7515 CNRS, ECPMULP,

25, rue Becquerel, 67087 Strasbourg Cedex 02, France

[d] Laboratoire d'Ingénierie Moléculaire Analytique, IPHC, UMR7178, ECPM,

25 rue Becquerel, 67087 Strasbourg Cedex 02, France

Supporting information for this article is available on the WWW under <http://dx.doi.org/10.1002/ejic.200900251>.

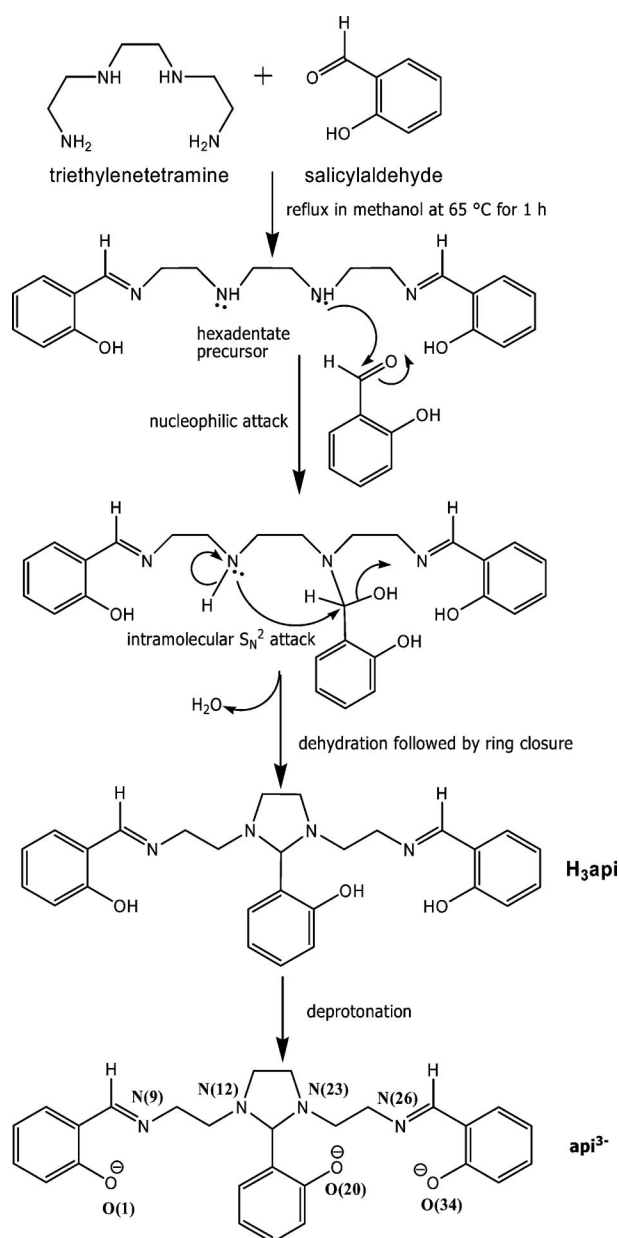
macrocyclic complexes with a lower $\rho = 1:1$. This dependency of the Ln^{3+} dinucleation process on ρ is reasonable because of the hard Lewis acidity of Ln^{3+} ions. So, ρ could indeed be an important molecular design parameter for new types of photonic devices and MRI contrast agents which take advantage of the tunable co-operative electronic behaviour of Ln^{3+} - Ln^{3+} couples. Thus, binuclear complexes are expected when the tendency of lanthanide ions to form species having higher coordination numbers is combined with the well-known ability of Schiff bases to bridge multiple metal centers. Considerable work has been concentrated in this line with N,N' -ethylene-bis(salicylideneimine) or H_2salen .^[36] Depending on the preparative procedures, a number of $\text{Ln}^{\text{III}}\text{-H}_2\text{salen}$ complexes with different compositions have been reported till now, including $\text{Ln}_2(\text{salen})_3$, $[\text{Ln}_2(\text{H}_2\text{salen})_3(\text{NO}_3)_4](\text{NO}_3)_2 \cdot 3\text{H}_2\text{O}$, $\text{Eu}(\text{Hsalen})(\text{salen})$, $\text{Ln}(\text{H}_2\text{salen})\text{X}_3 \cdot n\text{H}_2\text{O}$ ^[37–39] etc. These complexes are stable enough under physiological conditions. However, the literature is quite scarce in dealing with the various aspects involving different physical and photochemical properties. Especially neutral low-coordination number lanthanide complexes, devoid of coordinated solvents and salts, are interesting because they can provide open metal coordination sites for performing useful chemical transformations on organic substrates. Chemists now have realized that it is essential to design appropriate ligands to optimize the luminescence properties of lanthanide ions by facilitating the well-known light conversion, which actually is an efficient ligand-to-metal energy transfer process.

In an effort to gain more insight into the relationship between the ligand structure and, also, to unravel suitable synthons for the preparation of chelating ligands, we have turned our attention to the synthesis of multidentate ligand api^{3-} designed to encapsulate judiciously chosen lanthanide ions. The synthesis and characterization of a potentially heptadentate N_4O_3 donor acyclic Schiff base, H_3api , as well as two of its neutral homodinuclear complexes with Pr^{3+} and Nd^{3+} are reported. Structures of both the complexes have been invariably established from single-crystal X-ray diffraction. Interesting photoluminescence properties have been explored through detailed photophysical investigation and it shows that the flexible Schiff base can enhance the luminescence in the complexes by providing proper conjugate absorption groups for suitable energy transfer.

Results and Discussion

The Schiff base was prepared following the literature procedure with a slight modification.^[40] The reaction of triethylenetetramine and salicylaldehyde in 1:3 molar ratio in methanol affords the μ -bis(tetradentate) ligand H_3api through the formation of an imidazolidine ring in place of the ethylenediamine part of the parent hexadentate precursor. This semi-rigid 2-hydroxyphenyl-substituted five-membered imidazolidine ring inside the ligand backbone acts as a spacer-cum-bridging-cum-heterocyclic backbone unit. Synthesis of H_3api had been achieved in a two step reaction

which was initiated by an intermolecular nucleophilic attack on the incoming salicylaldehyde carbon atom by imine nitrogen of the parent hexadentate ligand as shown in Scheme 1. In the second step of the reaction, the intramolecular rearrangement (via $\text{S}_{\text{N}}2$ attack) takes place which finally introduces the imidazolidine ring through an alkylating cyclization process centred on the two secondary amine functions of the intermediate species. A plausible mechanism for this reaction leading to the final H_3api ligand is given in Scheme 1. Because each ligand carries a triple negative charge, the positive charge of the two trivalent lanthanide ions is counterbalanced and the dinuclear complexes are neutral; therefore no counterions are necessary. This is in contrast with the $f-d$ complexes with salen-type



Scheme 1. Probable mechanism for the formation of the H_3api ligand.

ligands, the lanthanide complexes with salicylaldehyde Schiff bases which have counterions such as nitrate groups or lipophilic bis(benzimidazole)pyridine-based ligands. The reasons why a dinuclear complex is formed instead of a mononuclear species are due to the tendency of the lanthanide(III) ions to achieve a high coordination number and to the nature of the ligand itself, auspicious to such a coordination mode (fused chelating parts). Typically, the coordination number of the trivalent lanthanide ions in coordination compounds is found eight or nine, though six-coordinate lanthanide(III) complexes are known, for example the tris(β -diketonato) lanthanide(III) complexes. The formation of the heptadentate Schiff base ligand H₃api containing pendant imidazolidine rings is supported by IR and mass spectroscopy. In the IR spectrum of the ligand the very strong band obtained at 1637 cm⁻¹ may be correlated to the C=N stretching frequency. The phenolic $\nu_{\text{str}}(\text{C}-\text{O})$ appeared at 1260 cm⁻¹. The presence of a sharp peak at 1112 cm⁻¹ confirms the formation of imidazolidine ring. Condensation of all the primary amine groups in the final ligand product is confirmed by the absence of the N-H stretching bands in the region 3150–3450 cm⁻¹. In mass spectrum the molecular ion peak (m/z) is observed at 458, which indicates the formation of the desired imidazolidine Schiff base ligand.

Fourier Transform Infrared Spectra

The infrared spectra of both the complexes are fully consistent with their crystal structures established through the X-ray analyses. The FT-IR spectra of the complexes contain strong characteristic C=N bands. Upon coordination to the metal center, the imine C=N stretching frequency drops from 1637 cm⁻¹ in the free ligand to 1614 and 1610 cm⁻¹ in the Pr^{III} and Nd^{III} complexes, respectively, thus confirming the complexation of the lanthanide ions. Deprotonation of all phenolic functions is confirmed by the lack of O-H stretching bands in the region 2500–3500 cm⁻¹ for both the complexes. One bifurcated strong peak at 1540 cm⁻¹ can be attributed to the vibration of the phenoxy oxygen atoms present in two different environments. Ligand coordination to the Ln^{III} metal center is substantiated by two bands at 462 and 448 cm⁻¹ corresponding to $\nu_{\text{str}}(\text{Ln}-\text{N})$ and $\nu_{\text{str}}(\text{Ln}-\text{O})$, respectively, however, assignments of these bands are very difficult in this region because of the low energies associated with these vibrations. All the above observations are similar to those of the previously reported alike complexes.^[41] The infrared spectrum of [Pr(api)]₂ was almost superimposable in the 1400–1700 cm⁻¹ region with that of [Nd(api)]₂, suggesting the isostructural nature of the complexes.

Crystal Structure Descriptions of [Pr(api)]₂ (1) and [Nd(api)]₂ (2)

The X-ray analysis reveals the complexes to be isostructural, both being centrosymmetric in nature. Labeled

ORTEP diagrams of **1** and **2** have been shown in the Figures 1 and 2 respectively. In the complex, the ligand has approximate non-crystallographic C_s symmetry about a plane that bisects the central “imidazolidine” ring and includes the attached phenolate ring oriented essentially orthogonally to the imidazolidine ring. The four ligand nitrogen atoms lie in a plane within 0.01 Å and the two terminal phenolate rings are inclined by ca. 26° to this plane. The potentially heptadentate ligand api³⁻ (see Scheme 1) contains three strong donors, namely phenoxo oxygen atoms as well as four weak donors (two imine and two imidazolidine N atoms) providing excellent coordination ability with inner-transition metal ions. The ligand together with a centrosymmetrically related counterpart utilize all of their potential co-ordinating sites to result the homodinuclear Ln^{III} complexes (Ln = Pr and Nd for **1** and **2**, respectively). Instead of forcing N₄O₃ donor atoms exclusively from one ligand onto one metal ion as reported for the encapsulated dimers,^[42] here the homodinuclear complexes contain two lanthanide ions where each of the metal ions is coordinated by two N₂O donor sets, each coming from one ligand. Two phenolate oxygen atoms, from the middle arm of each ligand, act as μ -bridges between the two metal centers and complete the eight-membered coordination sphere, overall furnishing a sandwich type dimeric structure. Generally there are three geometries reported to an eight-coordinate metal ion: cube, square antiprism, and dodecahedron. All of these forms are energetically very similar and the cube can be easily distorted to an antiprism or dodecahedron by interligand repulsion or ligand backbone *gauche* strain;^[43] generally steric nonrigidity is observed. The two Ln^{III} and two bridging oxygen atoms form a planar four-membered ring with a metal–metal separation of about 3.949 Å, and angles at the oxygen-bridgehead of 109.35 in **1** and 109.88(2)° in **2**. The shorter Ln^{III}–Ln^{III} separation in this dinuclear complex, compared to that of macrocyclic crown ether type of complexes, is probably largely due to the reduction in Ln^{III} coordination from ten to twelve in those macro complexes to eight in the reported one with a consequent “opening up” of the bond angles at each Ln^{III} cation. The geometry around each lanthanide atom can be viewed as a distorted square antiprism, in which one square is composed of donor atoms O(20) from middle arm phenoxy, O(34) from terminal phenoxy, N(23) imidazolidine nitrogen, N(26) imine nitrogen, and the other of O(20), O(1), N(12), and N(9) from the similar locations respectively. The Ln–N(imidazolidine) bond lengths are approximately 0.3 Å larger than the Ln–N(imine) bond lengths in all the cases. Since the bridging oxygen atoms O(20) form two strong Ln–O bonds, their basicity should be lowered relative to that of the singly phenoxy O atoms. Observed average Ln–O(singly phenoxy) bond lengths are shorter by 0.110 Å than the Ln–O(bridgehead) bond lengths, which is quite common in these kind of systems. The local coordination environment is exactly identical for all the metal centers with LnN₄O₄ chromophore. Coming on to the ligand, the five-membered imidazolidine ring adopts an envelope conformation with C(21) lying out of the plane defined by

N(12), N(23), C(13), and C(22). Both N(23)–C(24)–C(25)–N(26) and N(12)–C(11)–C(10)–N(9) adopt *gauche* conformations [torsion angles: N(12)–C(11)–C(10)–N(9) $-175.5(3)^\circ$; N(23)–C(24)–C(25)–N(26) $-178.7(1)^\circ$]. The overall ligand shape resembles the capital letter T. Due to the presence of several saturated sp^3 -hybridised C atoms in the amine part, the ligand loses the planarity and induces the Ln^{III} centers to enjoy a distorted square antiprism geometry with distortions in bond angles and distances (allowing for ionic size differences) of roughly similar magnitudes. The two coordination polyhedra are edge linked about the O(20)⋯O(20*) vector (2.73 Å) (Figure 3) with an intramolecular Ln⋯Ln separation of about 3.949 Å. The shortest inter-dimer Ln⋯Ln distance is 9.58 Å. An inspection of the packing of the dimers reveals only weak π -stacking (3.5 Å interplanar separation) between the terminal phenolate rings of adjacent molecules, the overall intermolecular interactions being essentially van der Waals in nature.

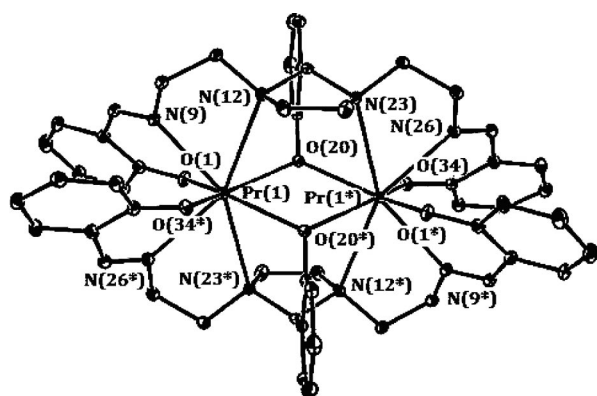


Figure 1. ORTEP diagram of **1** with displacement ellipsoids drawn at the 50% probability level. H atoms are omitted for clarity. * Symmetry code to the equivalent positions: $2 - x, -y, 2 - z$.

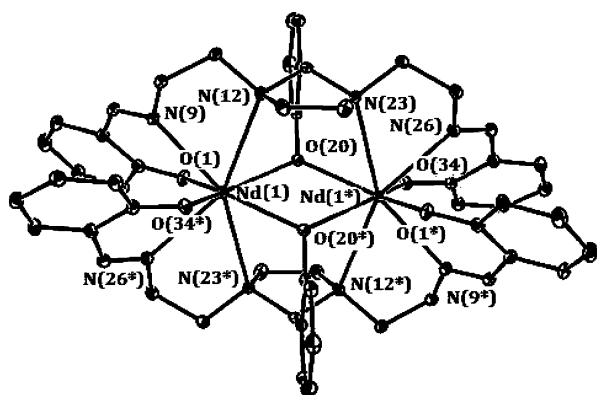


Figure 2. ORTEP diagram of **2** with displacement ellipsoids drawn at the 50% probability level. H atoms are omitted for clarity. * Symmetry code to the equivalent positions: $2 - x, -y, 2 - z$.

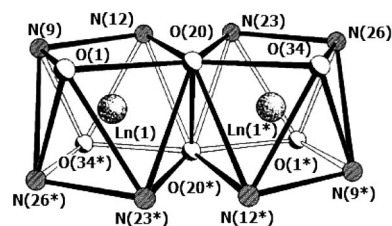


Figure 3. The distorted square antiprism coordination environment around the Ln^{III} ion.

All the data obtained are consistent with those found in the eight-coordinated La^{III} complexes of *N*-[2-(dimethylamino)ethyl]salicylideneamine^[44] and 1,4,7,10-tetrakis(2-carbamoyl ethyl)-1,4,7,10-tetraazacyclododecane.^[45] Although the formation of a dinuclear structure is not a surprise, this open-sandwich-like structure is unexpected. This no doubt arises from the rigid five-membered imidazolidine ring in the ligand backbone but also forces the ligand into a more open configuration rendering impossible the coordination of all the donor atoms of one ligand to one metal ion. Instead, these two ligands cooperate with each other to form two compartments to accommodate two metal ions. Detailed bonding study does not reveal any trace of intermolecular weak or hydrogen bonding interactions within the system (Figure 4). A few selected bonding parameters are provided in Tables 1 and 2.

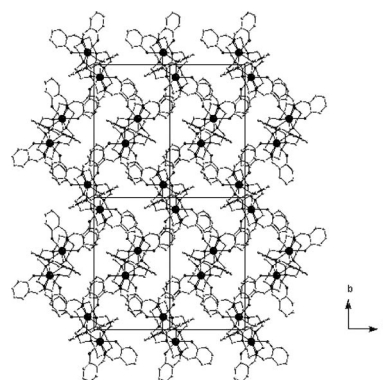


Figure 4. The packing view of [Ln(ami)]₂ in the $-ab$ plane.

Table 1. Comparison of the bond lengths [Å] in the complexes.

Bonds	1	2
Ln(1)–N(9)	2.578(4)	2.565(6)
Ln(1)–N(12)	2.873(5)	2.854(6)
Ln(1)–O(1)	2.303(4)	2.299(6)
Ln(1)–O(20)	2.436(3)	2.425(5)
Ln(1)–N(26*)	2.555(5)	2.545(6)
Ln(1)–N(23*)	2.854(5)	2.840(6)
Ln(1)–O(34*)	2.326(3)	2.309(4)
Ln(1)–O(20*)	2.418(4)	2.400(6)

Symmetry code (*): $2 - x, -y, 2 - z$

Table 2. Comparison of the bond angles [°] in the complexes.

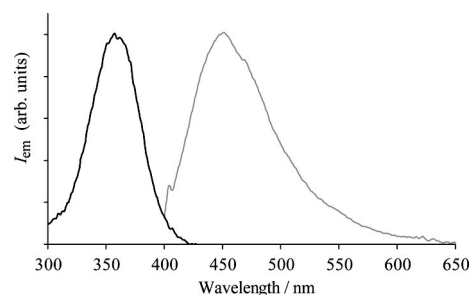
Bond angles	1	2
O(1)–Ln(1)–O(20)	82.14(13)	81.59(19)
O(1)–Ln(1)–N(9)	70.54(15)	70.8(2)
O(1)–Ln(1)–N(12)	111.41(14)	111.24(19)
O(1)–Ln(1)–O(20*)	141.83(13)	141.43(18)
O(1)–Ln(1)–O(34*)	130.32(14)	131.5(2)
O(1)–Ln(1)–N(23*)	81.91(14)	81.67(18)
O(1)–Ln(1)–N(26*)	73.60(16)	74.0(2)
O(20)–Ln(1)–N(9)	110.03(13)	110.94(18)
O(20)–Ln(1)–N(12)	69.41(12)	69.62(16)
O(20)–Ln(1)–O(20*)	70.65(12)	70.12(17)
O(20)–Ln(1)–O(34*)	144.43(12)	144.03(19)
O(20)–Ln(1)–N(23*)	83.85(12)	83.21(16)
O(20)–Ln(1)–N(26*)	142.53(15)	142.39(19)
N(9)–Ln(1)–N(12)	64.01(12)	64.61(17)
O(20*)–Ln(1)–N(9)	143.61(12)	143.51(18)
O(34*)–Ln(1)–N(9)	75.24(13)	75.28(19)
N(9)–Ln(1)–N(23*)	146.46(12)	146.13(17)
N(9)–Ln(1)–N(26*)	88.50(15)	87.7(2)
O(20*)–Ln(1)–N(12)	83.94(12)	83.36(16)
O(34*)–Ln(1)–N(12)	83.16(13)	83.00(17)
N(12)–Ln(1)–N(23*)	147.33(11)	147.04(16)
N(12)–Ln(1)–N(26*)	146.28(15)	146.21(19)
O(20*)–Ln(1)–O(34*)	84.72(12)	84.30(17)
O(20*)–Ln(1)–N(23*)	69.30(11)	69.71(16)
O(20*)–Ln(1)–N(26*)	113.25(14)	113.94(19)
O(34*)–Ln(1)–N(23*)	111.54(13)	111.76(16)
O(34*)–Ln(1)–N(26*)	70.55(15)	70.9(2)
N(23*)–Ln(1)–N(26*)	65.06(14)	65.47(19)

Symmetry code (*): 2 – x, –y, 2 – z

Table 3. Photophysical properties of the ligand in methanol.

Absorption	Emission	
λ_{max} (ε)	λ_{max}	$\tau_{\text{fluor.}}$ / ns
313 nm (5150 M ⁻¹ cm ⁻¹)	452 nm	3.9 (71%)
401 nm (1750 M ⁻¹ cm ⁻¹)		0.7 (21%)

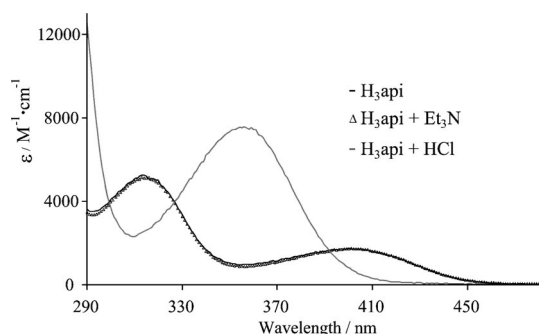
Upon excitation into the UV region, the fluorescence spectra of the ligand display a pronounced emission band with maximum at 452 nm (Figure 6). Surprisingly, the corresponding excitation spectrum (Figure 6) displayed the maxima to be at 357 nm, a region corresponding to a well in the absorption spectra. The corresponding Stokes shift is very large (ca. 5800 cm⁻¹), indicating a large electronic reorganization between the ground and excited states. The fluorescence lifetimes of the emission of the ligands are in the nanosecond regime, suggesting emission from a singlet state.

Figure 6. Fluorescence (grey line, $\lambda_{\text{exc}} = 360$ nm) and excitation (black line, $\lambda_{\text{em}} = 450$ nm) spectra of the ligand in methanol.

UV/Vis Spectroscopy and Photoluminescence Studies

Photophysical Properties of the Ligand

Figure 5 displays the UV/Vis absorption spectra of the H₃api ligand in methanol and its main photophysical properties are given in Table 3. The absorption spectrum of the ligand is composed of two main absorption bands. The high energy one (313 nm), is associated to $\pi \rightarrow \pi^*$ transitions centred on the benzene moiety. The assignment of the low energy band is more speculative, but on the basis of its medium absorption coefficient, it may have a pronounced character of $n \rightarrow \pi^*$ transition.

Figure 5. UV/Vis absorption spectra of the ligand (2×10^{-4} M in methanol; black line); ligand containing Et₃N (10 μL in 2 mL of a 2×10^{-4} M solution in methanol; triangles) and ligand containing HCl (10 μL in 2 mL of a 2×10^{-4} M solution in methanol; grey line).

In order to understand the origin of the emission band and its excitation spectrum, the absorption spectra of ligand in different acido-basic conditions were recorded (Figure 5). While the absorption spectra of ligand are essentially unchanged in the presence of Et₃N, the presence of concentrated aqueous HCl results in the appearance of a strong absorption band at 356 nm, corresponding to the region of maximum excitation observed above. The emission spectra upon acidification and basification of the solution of the ligand are given in Figure S1 (see Supporting Information). In acidic conditions, and to a lesser extent in basic ones, the corresponding fluorescence spectra show a marked decrease of the fluorescence intensity, indicating that the observed fluorescence is probably originating from a deprotonated state of the phenolic residues. In the absence of base, a possible origin of the emission may be found in the presence of an intramolecular proton transfer excited state, implicating the aminal function and probably favoured by the higher acidity of phenol/naphthol functions in the excited state.

Solid-State Photoluminescence Spectra of 1 and 2

The emission spectrum of the complex **1** is shown in Figure 7. It presents two characteristic emission regions, those corresponding to the $^1D_2 \rightarrow ^3F_J$ ($J = 2$ to 4) in the 900–1150 nm range and those corresponding to the $^1G_4 \rightarrow ^3H_J$ (J

= 4–6) above 1250 nm.^[46] The luminescence lifetime of the Pr excited state was monitored at 900 nm following pulsed excitation at 300 nm. The decay curves can not be conveniently fitted with a single exponential and it was necessary to introduce two lifetimes in the fitting process. After measuring the decay of the luminescence intensity upon excitation with the pulsed Xenon lamp, the decay was first corrected for the excitation function using a scattering solution and this corrected decay was subjected to the deconvolution process. The decays were fitted with mono- and bi-exponential functions, showing in all our cases a better fit with bi-exponential ones. From these fittings, the relative populations of the two components were determined. The fitted lifetimes were 8.0 and less than 0.5 μ s (corresponding to the limit of accuracy) respectively, corresponding to 40 and 60% of the total emitted intensity. This fact points to the presence of two distinct Pr sites within the complex (confirmed by the single-crystal X-ray diffraction data).

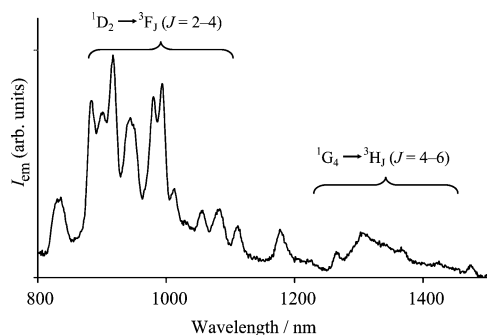


Figure 7. NIR emission spectrum ($\lambda_{\text{exc}} = 300$ nm, cut-off filter at 645 nm) of **1** in the solid state at 298 K.

The emission spectrum of the Nd complex was similarly measured in the solid state (see Figure 8). The emission bands observed in the NIR emission spectra of the Nd complex can be safely ascribed to the ${}^4F_{3/2} \rightarrow {}^4I_J$ transitions of Nd at $\lambda = 850\text{--}950$ nm ($J = 9/2$), $1050\text{--}1150$ nm ($J = 11/2$) and $1300\text{--}1400$ nm ($J = 13/2$).^[47] Between 980 and 995 nm, one can also observe two weak emission bands, the origin of which may be found in the mixture of emission arising from the higher energy ${}^2H_{9/2}$ level of Nd. The excited-state lifetime of Nd was monitored at 1060 nm upon excitation at 300 nm, but appeared too short (<1 μ s) to be measured with our experimental setup.

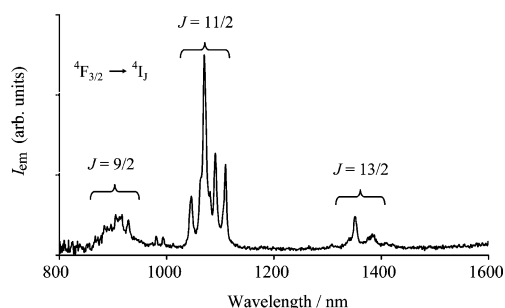


Figure 8. NIR emission spectrum ($\lambda_{\text{exc}} = 300$ nm, cut-off filter at 645 nm) of **2** in the solid state at 298 K.

The excitation spectra of the complexes have also been recorded. The representative excitation spectrum of the Pr complex in the solid state is shown in Figure 9. Recording emission at 894 nm with 10-nm slits at both the excitation and the emission, one can observe a broad and unstructured band with a maximum at $\lambda \approx 350$ nm, attributed to a ligand-centred sensitization process. Nevertheless, one can also observe two sharper excitation bands at 297 and 468 nm. From their narrow shapes, we can potentially attribute such bands to direct excitation of the f electronic states, pointing to a rather low efficiency of the ligand-based photosensitization process, as often observed with NIR emitting compounds.

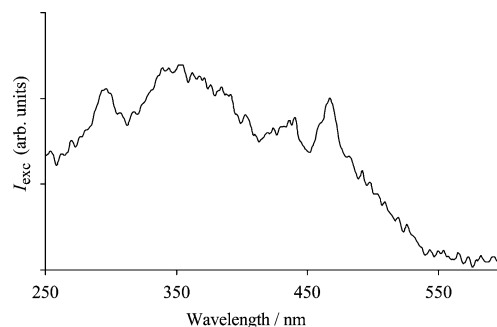


Figure 9. Excitation spectrum of the Pr complex ($\lambda_{\text{em}} = 884$ nm, high-pass filter at 645 nm).

Conclusion

In the present work a functionally dinucleating μ -bis(teradentate)-type ligand $H_3\text{api}$ incorporating amine, imine, and phenol functions has been synthesized and characterized. It is noteworthy that in the Schiff base a five-membered imidazolidine ring is formed at the backbone after the condensation and that the middle arm is therefore unique from the other two arms. The one-pot reactions with $\text{Ln}(\text{NO}_3)_3$ salts furnish two new doubly phenoxo-bridged centrosymmetric homodinuclear Pr^{III} and Nd^{III} complexes where all the metal ions adopt a distorted square antiprism coordination. The single-crystal X-ray diffraction studies reveal interesting chelating and bridging modes of the heptadentate ligand leading to the open-sandwich-like structures of the complexes. Detailed photophysical investigations of the ligand along with the solid-state photoluminescence spectroscopic studies on both the complexes were carried out. The complexes give emission bands in the near infrared region. Further work is being directed toward the synthesis of lanthanide coordination networks using new chelating ligands with different backbones and cavities, and to explore their luminescence properties as well as potential application as novel tunable photonic devices.

Experimental Section

General Remarks: Elemental analyses (C, H and N) were performed on a Perkin–Elmer 2400 CHN Elemental Analyser. The mass spec-

trum was obtained with a Kratos MS 50 (Electron-Impact ionization, EI). The FT-IR were recorded on a Perkin-Elmer RX 1 FT-IR spectrophotometer in the range 4000–200 cm^{-1} as a solid KBr disc. Fluorescence spectra in solutions were measured in 1- cm^2 quartz (Suprasil) cells on a FL 920 Edinburgh Instrument equipped with a Hamamatsu R928 photomultiplier for the visible domain. Steady state measurements were performed using a 450-W Xenon arc lamp while fluorescence lifetimes were determined in the TCSPC mode using a variable-frequency picosecond-pulsed LED ($\lambda = 310 \text{ nm}$). Decay curve were deconvoluted by using the program provided by the supplier, using a solution of silica suspended in water for the measurement of the scattered light. Absorption spectra were recorded in 1- cm^2 quartz (Suprasil) cuvettes on a Shimadzu UV3600 spectrometer at concentrations of $2 \times 10^{-4} \text{ M}$ in UV-grade methanol. NIR emission spectra were measured as solid samples in 2 mm diameter quartz tubes on the same instrument using a liquid nitrogen-cooled Hamamatsu R5509-72 photomultiplier. Steady state measurements were performed using a 450-W Xenon arc lamp, while lifetimes were determined by means of a pulsed Xenon flash lamp.

Syntheses: All the chemicals and solvents used for this synthesis were of analytical reagent grade. Salicylaldehyde, triethylenetetramine (trien) (99% pure), $\text{Pr}(\text{NO}_3)_3 \cdot 6\text{H}_2\text{O}$ (99.99% pure), $\text{Nd}(\text{NO}_3)_3 \cdot 6\text{H}_2\text{O}$ (99.99% pure) were purchased from Aldrich Chemical Co. Inc. and used as received without further purification.

Synthesis of the Schiff Base Ligand H_3api : 3 mmol salicylaldehyde dissolved in 10 mL of methanol was mixed with 10 mL of methanolic solution of 1 mmol triethylenetetramine and the mixture was refluxed at 65 $^\circ\text{C}$ for 1 h (Scheme 1). The resulting deep yellow solution containing the Schiff base ligand was cooled overnight to yield fine needle-shaped crystals of the ligand. The product was collected by filtration, washed with diethyl ether and dried at room temperature; yield 8.6 g (95%); m.p. 101–103 $^\circ\text{C}$. $\text{C}_{27}\text{H}_{30}\text{N}_4\text{O}_3$ (458.5): calcd. C 70.72, H 6.59, N 12.22; found C 70.60, H 6.52, N 12.10. ESI-MS (amu): $m/z = 458 [\text{H}_3\text{api}^+]$.

Syntheses of the Complexes

$[\text{Pr}(\text{api})_2]$ (1): To a 25 mL of methanolic solution of $\text{Pr}(\text{NO}_3)_3 \cdot 6\text{H}_2\text{O}$ (0.435 g, 1 mmol), 15 mL of methanolic solution of the 2 mmol Schiff base ligand H_3api was slowly added. The mixture was stirred for 10 min, followed by reflux for additional 35 min. The resulting mixture was filtered and the final filtrate was kept undisturbed for overnight at room temperature. Pale green rod-shaped crystals were obtained by slow evaporation of the filtrate solution. Suitable X-ray diffraction-quality single-crystals were mechanically isolated from the bulk materials; yield 85%. $\text{C}_{54}\text{H}_{54}\text{N}_8\text{O}_6\text{Pr}_2$ (1191.27): calcd. C 54.37, H 4.56, N 9.39; found C 54.30, H 4.60, N 9.42.

$[\text{Nd}(\text{api})_2]$ (2): The synthetic procedure is exactly the same as that of the previous complex except 0.359 g (1 mmol) $\text{Nd}(\text{NO}_3)_3 \cdot 6\text{H}_2\text{O}$ was taken in 25 mL of methanol in the place of Pr-salt. Colourless rhombic shaped crystals were obtained by slow evaporation of the final filtrate after one day. X-ray diffraction-quality single-crystals were mechanically isolated from the bulk materials collected after filtration and drying; yield 82%. $\text{C}_{54}\text{H}_{54}\text{N}_8\text{Nd}_2\text{O}_6$ (1199.55): calcd. C 54.07, H 4.54, N 9.34; found C 54.10, H 4.62, N 9.28.

X-Ray Crystallographic Data Collection and Structure Refinements: Crystal data and details of the structure refinements are summarised in Table 4.

Table 4. Crystal data and structure refinement details for the complexes.

	1	2
Empirical Formula	$\text{C}_{27}\text{H}_{27}\text{N}_4\text{O}_3\text{Pr}$	$\text{C}_{27}\text{H}_{27}\text{N}_4\text{NdO}_3$
Formula weight	1191.27	1199.55
Crystal dimension /mm	$0.05 \times 0.09 \times 0.11$	$0.11 \times 0.21 \times 0.22$
Crystal System	monoclinic	monoclinic
Space group	$P2_1/n$ (No. 14)	$P2_1/n$ (No. 14)
$a / \text{Å}$	10.9129(4)	10.9571(3)
$b / \text{Å}$	18.9350(4)	18.9001(6)
$c / \text{Å}$	11.8972(4)	11.8356(4)
$\beta / ^\circ$	97.109(1)	96.956(2)
$V / \text{Å}^3$	2439.49(13)	2433.00(13)
Z	2	2
T / K	293	293
$\lambda_{\text{Mo-K}\alpha} / \text{Å}$	0.71073	0.71073
$D_c / \text{g cm}^{-3}$	1.624	1.637
μ / mm^{-1}	2.034	2.171
$F(000)$	1200	1204
θ range for data collection	2.0–27.9 $^\circ$	2.0–27.9 $^\circ$
Total data	11171	10805
Unique data	5810	5789
Observed data [$I > 3\sigma(I)$]	3470	3106
$R^{\text{[a]}}$	0.0398	0.0447
$R_w^{\text{[b]}}$	0.0848	0.1296
Goodness-of-fit, S	1.16	1.16
R_{int}	0.041	0.054
$\Delta\rho_{\text{max}} / e^{-\text{Å}^{-3}}$	1.72	1.73
$\Delta\rho_{\text{min}} / e^{-\text{Å}^{-3}}$	−0.69	−0.84

[a] $R = \Sigma(|F_o - F_c|) / \Sigma|F_o|$. [b] $R_w = \{\Sigma[w(|F_o - F_c|)^2] / \Sigma[w|F_o|^2]\}^{1/2}$.

$[\text{Pr}(\text{api})_2]$ (1) and $[\text{Nd}(\text{api})_2]$ (2): Each of a good quality air stable single crystal of **1** with dimension $0.05 \times 0.09 \times 0.11 \text{ mm}$ and **2** with dimension $0.11 \times 0.21 \times 0.22 \text{ mm}$ was mounted on a Nonius Kappa CCD diffractometer equipped with graphite-monochromated focused X-ray tube bearing a molybdenum target ($\text{Mo-K}\alpha$ radiation, $\lambda = 0.71073 \text{ Å}$). Data collection was performed using the software COLLECT. Frames were integrated and corrected for Lorentz and polarisation effects using DENZO. The scaling as well as the global refinement of crystal parameters was performed by SCALEPACK. Whole data processing was performed using the Kappa CCD analysis software.^[48] The structures have been solved by direct methods with SIR-92 program,^[49] combined to Fourier difference syntheses and refined against F using the CRYSTALS program.^[50] All non-hydrogen atoms were successfully refined with anisotropic thermal parameters. The H atoms were all located in a difference map, but those attached to carbon atoms were repositioned geometrically and refined with isotropic thermal parameters. All calculations and graphical works have been done by using WinGX,^[51,52] CAMERON^[53] and PLATON^[54] programs.

Supporting Information (see also the footnote on the first page of this article): Emission spectra of ligand H_3api after addition of Et_3N and HCl ($\lambda_{\text{exc}} = 360 \text{ nm}$).

CCDC-672293 (for **1**) and -672294 (for **2**) contain the supplementary crystallographic data for this paper. These data can be obtained free of charge from The Cambridge Crystallographic Data Centre via www.ccdc.cam.ac.uk/data_request/cif.

Acknowledgments

J. C. is thankful to the University Grants Commission, New Delhi for providing a senior research fellowship to him. S. T. is grateful to the Council of Scientific and Industrial Research, New Delhi

for a senior research fellowship grant [CSIR sanction number 09/096(0519)/2007-EMR-I].

- [1] P. Caravan, J. J. Ellison, T. J. McMurry, R. B. Lauffer, *Chem. Rev.* **1999**, *99*, 2293–2352.
- [2] J.-M. Lehn, *Angew. Chem. Int. Ed. Engl.* **1990**, *29*, 1304–1319.
- [3] J. Chakraborty, G. Pilet, M. S. El Fallah, J. Ribas, S. Mitra, *Inorg. Chem. Commun.* **2007**, *10*, 489–493.
- [4] S. W. A. Bligh, N. Choi, E. G. Evagorou, M. McPartlin, K. N. White, *J. Chem. Soc., Dalton Trans.* **2001**, *21*, 3169–3172.
- [5] C. S. Cutler, C. J. Smith, G. J. Ehrhardt, T. T. Tyler, S. S. Jurisson, E. Deutsch, *Cancer Biother. Radiopharm.* **2000**, *15*, 531–545.
- [6] B. M. Flanagan, P. V. Bernhardt, E. R. Krausz, S. R. Lüthi, M. J. Riley, *Inorg. Chem.* **2002**, *41*, 5024–5033.
- [7] S. Mizukami, H. Houjou, M. Kanetsato, K. Hiratani, *Chem. Eur. J.* **2003**, *9*, 1521–1528.
- [8] M. Kanetsato, S. Mizukami, H. Houjou, H. Tokuhisa, E. Koyama, Y. Nagawa, *J. Alloys Compd.* **2004**, *374*, 307–310.
- [9] N. Sabbatini, M. Guardigli, I. Manet, R. Ungaro, A. Casnati, R. Ziessel, G. Ulrich, Z. Asfari, J.-M. Lehn, *Pure Appl. Chem.* **1995**, *67*, 135–140.
- [10] P. L. Jones, A. J. Amoroso, J. C. Jeffery, J. A. McCleverty, E. Psillakis, L. H. Rees, M. D. Ward, *Inorg. Chem.* **1997**, *36*, 10–18.
- [11] J.-C. G. Bünzli, E. Moret, V. Foiret, K. J. Schenk, W. Mingzhao, J. Linpei, *J. Alloys Compd.* **1994**, *207*, 107–111.
- [12] M. Pietraszkiewicz, J. Karpiuk, A. K. Rout, *Pure Appl. Chem.* **1993**, *65*, 563–566.
- [13] J.-C. G. Bünzli, F. Ihringer, *Inorg. Chim. Acta* **1996**, *246*, 195–205.
- [14] H. Mikola, H. Takalo, I. Hemmilä, *Bioconj. Chem.* **1995**, *6*, 235–241.
- [15] G. F. de Sá, L. H. A. Nunes, Z.-M. Wang, G. R. Choppin, *J. Alloys Compd.* **1993**, *196*, 17–23.
- [16] M. P. Oude Wolbers, F. C. J. M. van Veggel, B. H. M. Snellink-Ruël, J. W. Hofstraat, F. A. J. Geurts, D. N. Reinhoudt, *J. Chem. Soc., Perkin Trans. 2* **1998**, 2141–2150.
- [17] W. D. Horrocks Jr., J. P. Bolender, W. D. Smith, R. M. Supkowski, *J. Am. Chem. Soc.* **1997**, *119*, 5972–5973.
- [18] M. H. V. Werts, J. W. Hofstraat, F. A. J. Geurts, J. W. Verhoeven, *Chem. Phys. Lett.* **1997**, *276*, 196–201.
- [19] S. Lange, I. Sildos, V. Kiisk, J. Aarik, *Mater. Sci. Eng. B* **2004**, *112*, 87–90.
- [20] A. Beeby, R. S. Dickens, S. Faulkner, D. Parker, J. A. G. Williams, *Chem. Commun.* **1997**, 1401–1402.
- [21] A. Beeby, S. Faulkner, *Chem. Phys. Lett.* **1997**, *266*, 116–122.
- [22] D.-J. Qian, H. Nakahara, K. Fukuda, K.-Z. Yang, *Langmuir* **1995**, *11*, 4491–4494.
- [23] R. Ludwig, H. Matsumoto, M. Takeshita, K. Ueda, S. Shinkai, *Supramol. Chem.* **1995**, *4*, 319–327.
- [24] O. A. Serra, E. J. Nassar, P. S. Calefi, I. L. V. Rosa, *J. Alloys Compd.* **1998**, *275*, 838–840.
- [25] G. Blasse, G. J. Dirksen, N. Sabbatini, S. Perathoner, *Inorg. Chim. Acta* **1987**, *133*, 167–173.
- [26] A. C. M. de Andrade, M. A. de Brito, A. L. Coelho, G. F. de Sa, *Inorg. Chim. Acta* **1976**, *19*, L19–L20.
- [27] I. A. Hemmilä, *Applications of Fluorescence in Immunoassays*, Wiley, New York, **1991**.
- [28] C. R. Ronda, *J. Alloys Compd.* **1995**, *225*, 534–538.
- [29] D. Parker, P. K. Senanayake, J. A. G. Williams, *J. Chem. Soc., Perkin Trans. 2* **1998**, 2129–2140.
- [30] J. Kido, W. Ikeda, M. Kimura, K. Nagai, *Jpn. J. Appl. Phys.* **1996**, *35*, L394–L396.
- [31] G. F. de Sá, S. Alves Jr., B. J. P. da Silva, E. F. da Silva Jr., *Opt. Mater.* **1998**, *11*, 23–28.
- [32] A. D. Garnovskii, A. L. Nivorozhkin, V. I. Minkin, *Coord. Chem. Rev.* **1993**, *126*, 1–69.
- [33] R. Gheorghe, M. Andruh, A. Müller, M. Schmidtman, *Inorg. Chem.* **2002**, *41*, 5314–5316.
- [34] A. M. Madalan, H. W. Roesky, M. Andruh, M. Noltemeyer, N. Stanica, *Chem. Commun.* **2002**, 1638–1639.
- [35] R. Gheorghe, M. Andruh, J.-P. Costes, B. Donnadieu, *Chem. Commun.* **2003**, 2778–2779.
- [36] R. D. Archer, H. Chen, L. C. Thompson, *Inorg. Chem.* **1998**, *37*, 2089–2095.
- [37] S. Afshar, J. I. Bullock, *Inorg. Chim. Acta* **1980**, *38*, 145–149.
- [38] W. Xie, M. J. Heeg, P. G. Wang, *Inorg. Chem.* **1999**, *38*, 2541–2543.
- [39] J. I. Bullock, H. A. Tajmir-Riahi, *J. Chem. Soc., Dalton Trans.* **1978**, 36–39.
- [40] T. Isobe, S. Kida, S. Misumi, *Bull. Chem. Soc. Jpn.* **1967**, *40*, 1862–1863.
- [41] J.-P. Costes, G. Novitchi, C. Lebrun, *J. Alloys Compd.* **2004**, *374*, 377–381.
- [42] S. Liu, L. Gelmini, S. J. Rettig, R. C. Thompson, C. Orvig, *J. Am. Chem. Soc.* **1992**, *114*, 6081–6087.
- [43] N. N. Greenwood, A. Earnshaw, *Chemistry of the Elements*, Pergamon Press: Oxford, England, **1984**.
- [44] P. Blech, C. Floriani, A. C. Villa, C. Guastini, *J. Chem. Soc., Dalton Trans.* **1990**, 3557–3561.
- [45] J. A. Morrow, S. Amin, C. H. Lake, M. R. Churchill, *Inorg. Chem.* **1993**, *32*, 4566–4572.
- [46] S. Comby, J.-C. G. Bünzli, *Handbook on the Physics and Chemistry of Rare Earth* (Eds.: K. A. Gschneider Jr., J.-C. G. Bünzli, V. Pecharsky), Elsevier B. V., Amsterdam, Vol. 37, Chap. 235, **2007**.
- [47] R. Ziessel, G. Ulrich, L. Charbonnière, D. Imbert, R. Scopelitti, J.-C. G. Bünzli, *Chem. Eur. J.* **2006**, *12*, 5060–5067.
- [48] *Nonius COLLECT, DENZO, SCALEPACK, SORTAV: KappaCCD Program Package*, Nonius B. V., Delft, The Netherlands, **1997–2001**.
- [49] *SIR92*, A new tool for crystal structure determination and refinement: A. Altomare, G. L. Casciaro, C. Giacovazzo, A. Guagliardi, M. C. Burla, G. Polidori, M. Camalli, *J. Appl. Crystallogr.* **1994**, *27*, 435–436.
- [50] D. J. Watkin, C. K. Prout, J. R. Carruthers, P. W. Betteridge, *CRYSTALS*, issue 11, Chemical Crystallography Laboratory, Oxford, UK, **1999**.
- [51] *WinGX*, A program for crystal structure analysis: L. J. Farrugia, *J. Appl. Crystallogr.* **1999**, *32*, 837–838.
- [52] *ORTEP-3 for Windows*, v. 2.02: L. J. Farrugia, *J. Appl. Crystallogr.* **1997**, *30*, 565.
- [53] D. J. Watkin, C. K. Prout, L. J. Pearce, *CAMERON*, Chemical Crystallography Laboratory, Oxford, UK, **1996**.
- [54] *PLATON for Windows*, v. 1.15: A. L. Spek, *Acta Crystallogr., Sect. A* **1990**, *46*, C34.

Received: March 17, 2009
Published Online: June 5, 2009